water

MDPI

Article

Spatiotemporal Characterization and Analysis of River Morphology Using Long-Term Landsat Imagery and Stream Power

Atefe Arfa-Fathollahkhani, Seyed Ali Ayyoubzadeh, Hossein Shafizadeh-Moghadam * and Hojjat Mianabadi *

Department of Water Engineering and Management, Tarbiat Modares University, Tehran 14977-13111, Iran
* Correspondence: h_shafizadeh@modares.ac.ir (H.S.-M.); hmianabadi@modares.ac.ir (H.M.); Tel.: +98-21-48292471 (H.S.-M. & H.M.)

Abstract: Meandering rivers are among the most dynamic Earth-surface systems, which generally appear in fertile valleys, the most valuable lands for agriculture and human settlement. Landsat time series and morphological parameters are complementary tools for exploring river dynamics. Karun River is the most effluent and largest meandering river in Iran, which keeps the Karun's basin economy, agriculture, and industrial sections alive; hence, investigating morphological changes in this river is essential. The morphological characteristics of Karun have undergone considerable changes over time due to several tectonic, hydrological, hydraulic, and anthropogenic factors. This study has identified and analyzed morphological changes in Karun River using a time series of Landsat imagery from 1985–2015. On that basis, morphological dynamics, including the river's active channel width, meander's neck length, water flow length, sinuosity index, and Cornice central angle, were quantitatively investigated. Additionally, the correlation between the stream power and morphological factors was explored using the data adopted from the hydrometric stations. The results show that the dominant pattern of the Karun River, due to the sinuosity coefficient, is meandering, and the majority of the river falls in the category of developed meander rivers. Moreover, the number of arteries reduced in an anabranch pattern, and the river has been migrating towards the downstream and eastern sides since 1985. This phenomenon disposes a change in the future that can be hazardous to the croplands and demands specific considerations for catchment management.

Keywords: Karun River; meander; stream power; Landsat; river morphology

check for updates

Citation: Arfa-Fathollahkhani, A.; Ayyoubzadeh, S.A.; Shafizadeh-Moghadam, H.; Mianabadi, H. Spatiotemporal Characterization and Analysis of River Morphology Using Long-Term Landsat Imagery and Stream Power. *Water* **2022**, *14*, 3656. https://doi.org/10.3390/w14223656

Academic Editor: Achim A. Beylich

Received: 3 August 2022
Accepted: 30 August 2022
Published: 13 November 2022

1. Introduction

Karun basin is one of the most critical basins in West Asia and the second most important river in the Persian Gulf and Oman Sea catchments. It is a river with greater discharge and the only navigable river in Iran with a critical role in the Karun basin's ecological, environmental, and socio-economic conditions. The river runs through several big cities such as Ahvaz, Shushtar, and Khorramshahr, with more than five million inhabitants. It is the main water supply for many agro-industries near the city of Ahvaz and for producing over 5.5 million tons/year of sugarcane. Therefore, monitoring the morphology and spatiotemporal dynamics of the Karun River is essential as a prerequisite for effective river management.

Meanders are the most common river pattern in populated areas [1], which are a response of the river to decrease its energy, whereas it leads to an increase in length and reduction in the channel's slope. Meandering rivers time and again occur in fertile valleys, the most valuable lands for agriculture and human settlement. Given that floodplains have been gradually occupied by growing urbanization and industrial development [2], this process increases the importance of flood control, bank erosion control, and meander migration. Therefore, investigating and revealing river path alteration trends are essen-

tial for assessing river dynamics, catchment management, risk reduction, and floodplain improvement [3,4].

Investigating the river path trend is feasible by studying the changes in morphological parameters of the river (e.g., width, wavelength, river length, sinuosity, and central angle). There is an extensive body of literature that has explored the linkage between the morphological characteristics and variables such as sediment rate, discharge fluctuation, river bed slope, climate change, gravel mining, dam construction, human interventions, and land use and land cover changes [5–15]. Riverbank erosion can lead to landscape degradation as well as environmental and socio-economic impacts, which have been observed in various countries at different scales [16]. Bank erosion and displacement of the river's path can result in river instability and meandering formation and development. In addition, human intervention in natural conditions and the riparian zone intensifies bank erosion [17–21]. As a result of human intervention, dam construction affects the downstream, which can seriously change the hydro-morphological characteristics such as sediment transport pattern and flow discharge, which cause riverbed run narrowing and bank erosion [22–27].

Stream power can be used to investigate the influence of flow discharge changes on river morphology [28]. Stream power, the product of discharge and the river's slope, is a helpful tool for describing the river's morphological changes [29,30]. Stream power has been less explored in the literature and was mainly considered concerning the bedload distribution [31], bank strength, prediction of channel dynamic [32], and sinuosity [33].

The bodies of water and river planform can be extracted through satellite images and using relevant spectral indices. Time series of satellite images paved the way for depicting the channel layout over time driven by natural events such as floods or anthropogenic activities [28]. Freely available satellite imagery with regular global coverage is a valuable resource for river monitoring. Although satellite imagery has a long-term archive, the spatial resolution of images has been increased over time, which is an essential factor, especially for monitoring narrow rivers. In many river studies, satellite images have been used for evaluating and monitoring river morphology [34–43].

Given the importance of the Karun River above, it is necessary to monitor the river's dynamics, for example, by examining and quantifying the geometry and pattern of the meanders over time. This paper investigates the trend of morphological changes of the Karun River and detects the underlying drivers over the last 30 years using Landsat imagery. In previous studies, the number of morphological characteristics was limited [44]; in this study, the sinuosity coefficient, central angle (Cornice angle), active channel width, wavelength, and river length, as well as arc properties, are analyzed. In addition, the river reach is categorized with three different methods (Schumm, Cornice, and Leopold), which have not been investigated previously. Finally, the relation between unit stream power (USP) and morphological parameters, essential for basin monitoring and management, will be quantified. These objectives, in conjunction, will help to understand how the changes in river flow discharge affect the river's morphological changes.

2. Material and Method

2.1. Study Area and Data

Karun River is located in the Karun basin with a catchment area of 67,112 km^2, which is characterized as the highest discharge and the longest river in Iran. The catchment is divided into three sub-basins and 42 plains (Table 1). With a total length of 950 km, Karun originates mainly from the Zardkuh Mountains of the Bakhtiari district and receives various tributaries such as Dez and the Kuhrang before passing through the city of Ahvaz and discharging into Arvandrud. In this study, a portion of the river with a length of 300 km (Figure 1) is investigated. Its upstream part is located close to one of the largest dams in Iran, Gotvand Dam, built in 2003, and the downstream region is located near the city of Shirinshahr. Several massive projects have been constructed since 70 years ago that show the socio-economic importance of this river [45]. Significant changes were imposed

on the river's morphology during these constructions; the most important outcomes were changing the river width and meanders.

Table 1. Details of Great Karun and its three sub-basins (Iran's Ministry of Energy, 2012).

Sub-Basin Name	Sub-Basin Code	Area (km^2)			Number of Fourth-Grade Sub-Basins	Main River
		Mountain	Plain	Total		
Karun	231	31,657.0	9538.7	41,195.7	30	Karun
Dez	232	14,893.1	5112.4	20,005.5	9	Dez
Karun downstream	233	28.5	5882.7	5911.2	3	Karun downstream
Great Karun basin	23	46,578.5	20,533.8	67,112.3	42	Great Karun

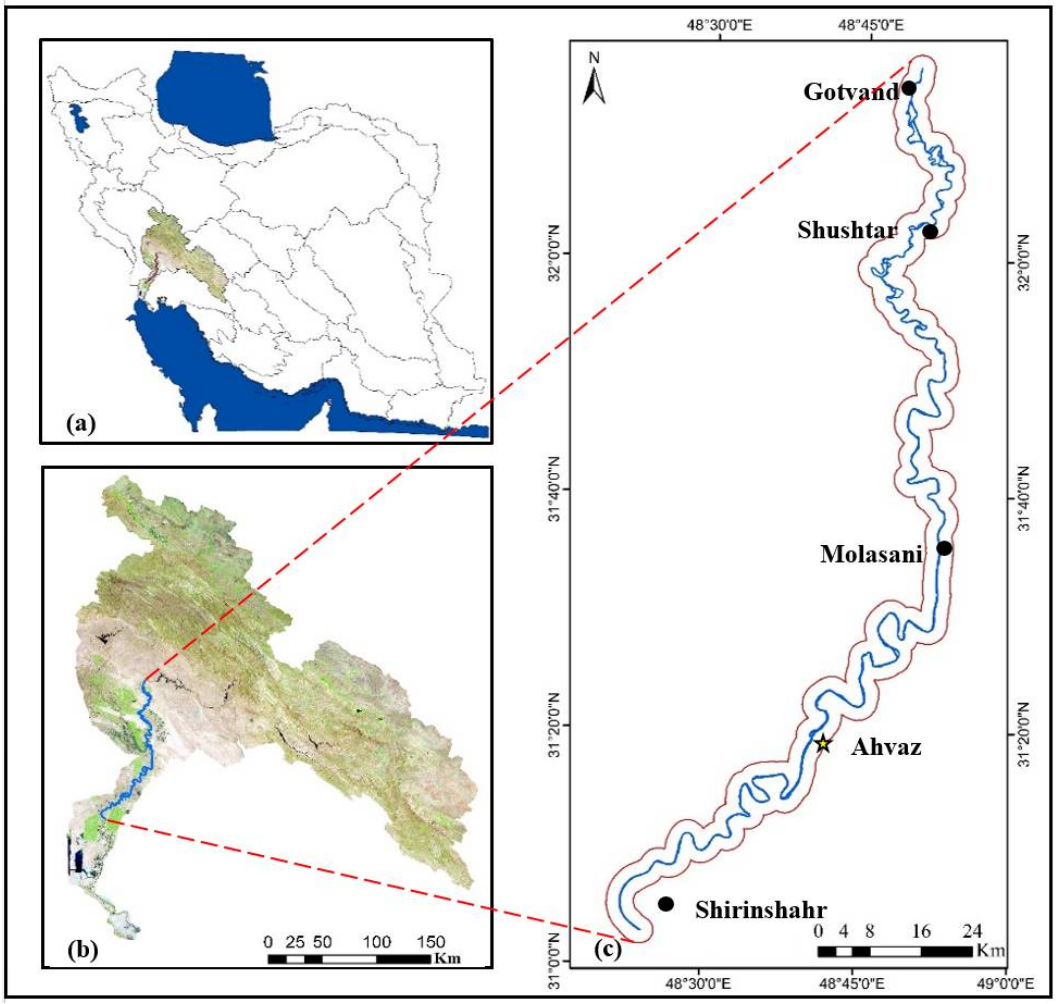

Figure 1. Study area in the Karun River basin. (**a**) Iran's second-grade catchment, (**b**) Great Karun catchment, (**c**) a river with a 3 km buffer zone (flow direction is north to south).

2.2. Data

Multi-temporal Landsat images were used to detect the dynamic of Karun River in three time points, namely, 1985, 2000, and 2015. To account for the topography of the region, a digital elevation model (DEM) with a resolution of one arc-second (30 m) was acquired from the SRTM satellite (Table 2, Figure 2—left panel). A land use map was extracted

from Landsat-8 in 2015 (Figure 2—right panel). Since the Karun River reaches its highest discharge in spring, the considered satellite data belonged to May. Three scenes of Landsat data have covered the study area.

Table 2. DEM and satellite data * to monitor the dynamic of Karun River.

Satellite	Sensor	Resolution (m^2)	Date
Landsat-4	TM	30 * 30	5 May 1985
Landsat-5	TM	30 * 30	30 May 2000
Landsat-8	ETM+	30 * 30	30 May 2015
SRTM		30 * 30	30 June 2018

* www.earthexplorer.gov (accessed on 10 April 2019).

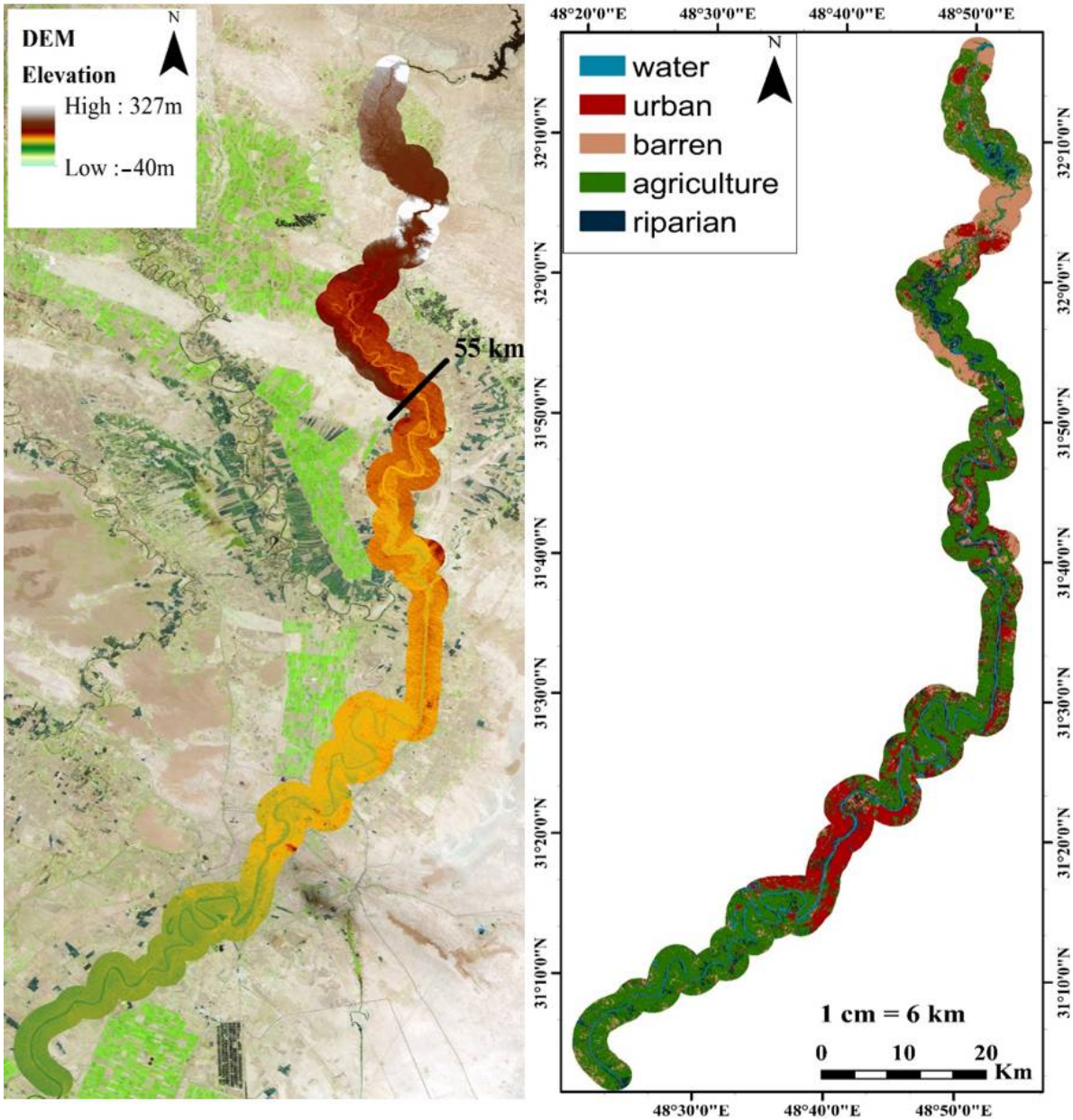

Figure 2. (**Left panel**) Digital elevation map of Karun Basin (SRTM). The 55 km segment is mentioned in the results section. (**Right panel**) Land use map of the study area extracted from Landsat data in 2015.

2.3. Methods

Landsat data with 15-year intervals (1985–2015) were processed to delineate the river's bed extent. The modified normalized difference water index (MNDWI) was employed to reveal the water body extents. MNDWI is a powerful remote sensing index for water body extraction [46]. MNDWI is computed using the near infrared and the short-wave infrared bands. Equation (1) shows the relation between NIR and SWIR for the calculation of MNDWI.

$$\text{MNDWI} = (\text{Green} - \text{SWIR})/(\text{Green} + \text{SWIR}) \quad (1)$$

A manual improvement followed the river's bed delineation; then, the centerline was extracted using the centerline function in ArcGIS. For a detailed exploration of the river, the study area was divided into eight segments based on Schumm's study in 1985, which categorizes the river's pattern according to three criteria: the number of courses, sinuosity coefficient (SC), and lateral stability (Figure 3).

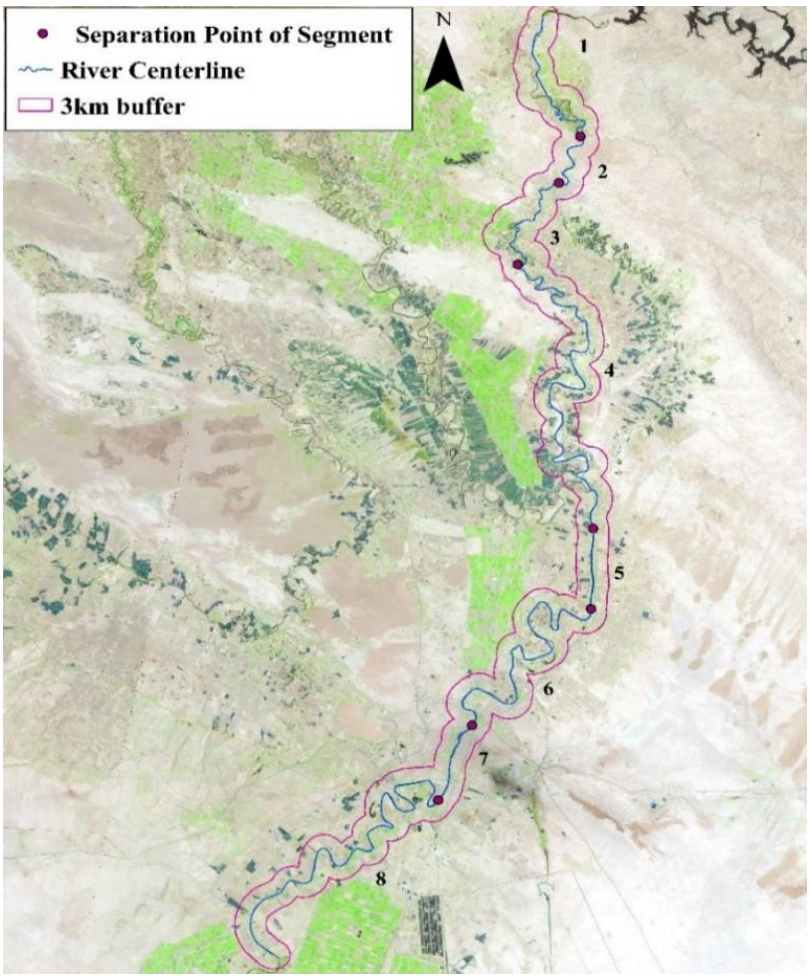

Figure 3. Segmentation of the study area for meandering characterization.

The SC and central angles are used to characterize meandering rivers [33,34,47,48]. The value of SC ranges between 1.5 and 4 [49–51]. Channels with an SC value of less than 1.05, from 1.06–1.3, and greater than 1.3 are called straight, sinuous, and meandering rivers [52]. The central angle was proposed by Cornice (1985). It works according to the central angle to quantify the extent of meandering development and distinguishing them in alluvial rivers (1980). Using the river route, morphological parameters were extracted for each time point as below:

Width: To obtain the river's width for each arc, four or five sections, including the beginning, end, and middle of the arc with different widths, were measured, and their average was introduced as a representative for each arc (Equation (2)).

$$\overline{B} = \sum_{i=1}^{i=n} B_i / n \tag{2}$$

Wavelength: For this purpose, inflection points (i) for each arc were determined, and the direct distance between each pair of points was measured as half of the wavelength because each wave consists of two arcs in the form of a sine function.

Central angle: The Cornice central angle indicates the river's form development, which can be deduced by enclosing a circle in an arc. In doing so, a circle is surrounded by an arc, then the first and endpoints of their connections are adjoined to the center of the circle; the angle created in the center is called the Cornice central angle.

Sinuosity: Sinuosity or the coefficient of curvature for each arc is the ratio of the river's length to half of the wavelength. For each arc, the length of the river's centerline was measured between the inflection points and half of the wavelength, which is the direct length between these points (Equation (3)).

$$\Omega = \frac{L_{r_{(i_1, i_2)}}}{\lambda / 2} \tag{3}$$

Slope: A digital elevation map (Figure 2—left panel) was used to calculate the slope for each arc. The points closest to the river (right and left bank of the arc) were identified, and their slope was calculated. According to Figure 4, the slope between three points (on each side of the arc) was calculated (Equations (4) and (5), and after averaging for each side, one slope was obtained, and an equivalent slope ($\overline{S}$) was extracted from the mean of the two values obtained for each side (Equation (6)).

$$S_{out} = \frac{S_1 + S_2}{2} + \frac{S_2 + S_3}{2} \tag{4}$$

$$S_{in} = \frac{S_4 + S_5}{2} + \frac{S_5 + S_6}{2} \tag{5}$$

$$\overline{S} = \frac{S_{out} + S_{in}}{2} \tag{6}$$

The hydraulic geometric flow discharge relation for the studied sections was obtained using the historical data. The relations between river discharge (Q) and some geometric (H, B, and A) and hydraulic parameters (V and τ) are shown in Figure 5. Flow parameters including H (average height), A (bed surface area), V (flow velocity), and τ (bed shear stress) were calculated based on observation in Ahvaz hydrometric station. Then, stream power per unit length, width, area, and weight were calculated using Equations (7)–(10).

$$\Omega = \gamma Q S, \tag{7}$$

$$\omega = \gamma Q H / B, \tag{8}$$

$$\eta / A = \tau V, \tag{9}$$

$$\eta / w = V S, \tag{10}$$

where γ is water-specific weight, Q denotes the river flow discharge, and S shows the longitudinal river's bed slope obtained from the DEM layer.

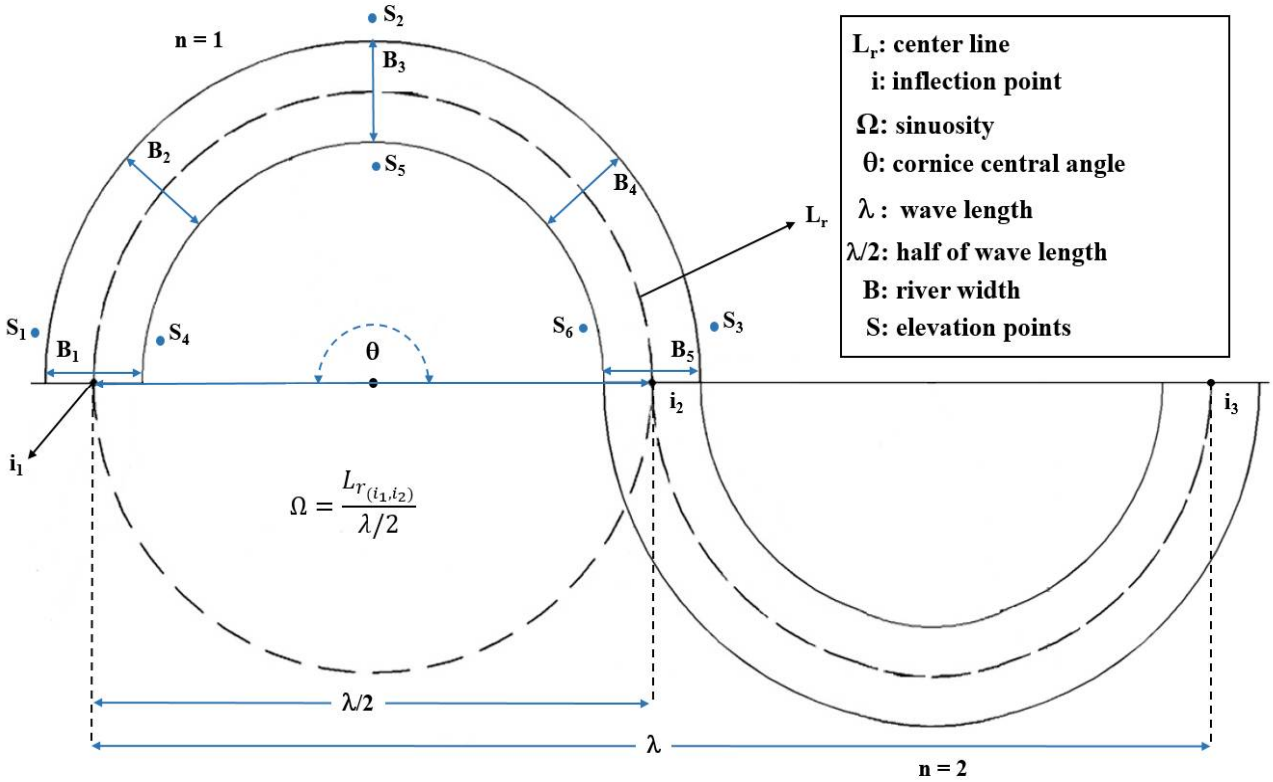

Figure 4. Calculation of the morphological parameters from satellite images.

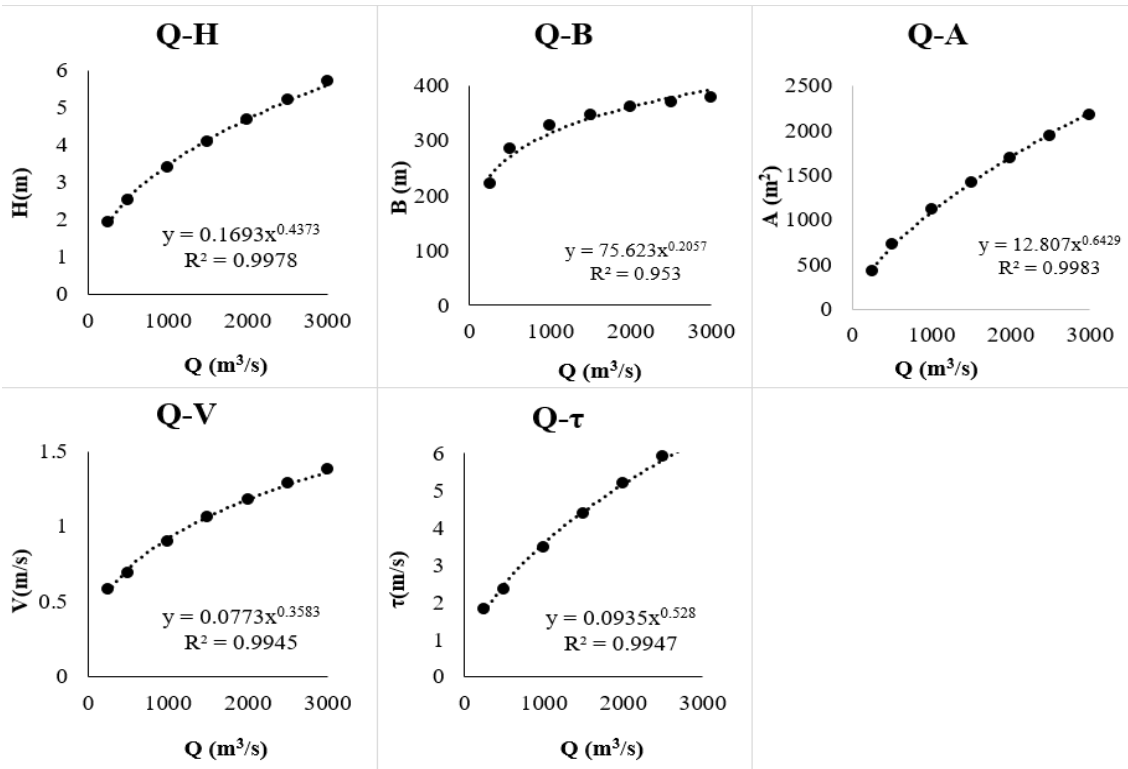

Figure 5. These graphs show the relationship between the river discharge and flow parameters in Ahvaz hydrometric station on the Karun River.

Morphological parameters and stream power have been calculated cumulatively across the study area. Since the integral for each parameter was converted to sigma, the distance between the arcs was assumed to be equal. As shown in Equations (11) and (12), X is the cumulative number of parameters that include the USP, morphological, hydraulic, and geometric parameters, x is the number of parameters in each arc, ds is equal, and n is the number of arcs along the river (Figure 4).

$$X = \int_0^{300} \overline{X}\, ds \tag{11}$$

$$X = \sum_1^{53} X_n \tag{12}$$

We use the normalized mass method to investigate the relationship between the UPS and morphological parameters of the river. Their graphs were drawn, the trend line with the best regression coefficient was plotted on each curve, and its equation was determined (1985, 2000, and 2015). Finally, the general relation was obtained. In the last step, the centerline of the river for each time point (1985, 2000, and 2015) was superimposed in AutoCAD, and common arcs were examined to determine the arc's migrations. Displacement and its clockwise angle relative to the north were calculated for each time interval (every 15 years and at the end of the last interval). Finally, the changes in the river's routes and the arcs with the highest migration were identified and analyzed.

3. Results

3.1. Schumm Approach for Channel Pattern

According to Schumm's channel classification scheme (1985), the Karun River demonstrated three primary forms: straight, meandering, and braided in the eight identified intervals. Table 3 summarizes the river's morphologic properties, whereas Tables 4 and 5 provide the temporal changing meandering and braiding development along the river path. As shown in Table 4, rotation and conversion are the dominant properties in the meandering segments, where segment 4 has the most active part. On the other hand, sinuous side channels, split channels, sub-parallel anabranches, and cutoff loops were the main properties of the braided patterns (Table 5).

Table 3. Properties of river pattern and changes in each interval.

Interval	Branches	Sinuosity Coefficient	Lateral Stability	Other Morphological Changes
1	Anabranch or Anastomosing	-	Arc rotation	Some arteries disappear—reduce width
2	Single-channel	Regular meander		Reduce width—meander neck displacement
3	Wandering	-	Main line change	Reduce width—some arteries disappear
	Anabranch or Anastomosing	-	Thalweg change	
4	Single-channel		Translation to downstream—neck and chute cutoff—increasing arc domain	Reduce width
	Wandering			
5	Single-channel	Straight		Reduce width
6	Single-channel		Translation to downstream	Reduce width
7	Single-channel	Straight		Reduce width
	Wandering			Reduce width
8	Single-channel		Translation to downstream	Reduce width
	Wandering			

Table 4. Observed changes are shown by (*) from 1985–2015 in the meandering pattern along Karun River based on Schumm's studies [53].

Interval	Meandering					
	Extension	Translation	Rotation	Conversion	Neck Cutoff	Chute Cutoffs
		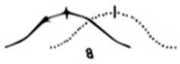				
1			Braiding			
2			*			
3						
4	*		*	*	*	
5			Straight			
6			*			
			Straight			
8			*	*		

Table 5. Observed changes are shown by (*) in the braided pattern along the Karun River in 30 years (1985–2015) in the braided pattern based on Schumm's studies [53].

Interval	Braided				
	Sinuous Side Channels Mainly	Cutoff Loops Mainly	Split Channel, Sinuous Anabranches	Split Channel, Sub-parallel Anabranches	Composite
					
1	*			*	
2			Meandering		
3	*	*			
4			Meandering		
5			Straight		
6			Meandering		
7			Straight		
8			Meandering		

* Observed changes.

3.2. Sinuosity Coefficient

Figure 6 demonstrates the changes in arc sinuosity along the river from Gotvand to Shirinshahr. As shown, after 55 km from the beginning of the reach, the river altitude decreases to 40 m, while the altitude variation within 300 km of the river is only 60 m, so the river proceeds with a gentle slope at the beginning of the reach. Based on Figures 2 and 7, the conclusion can be drawn that the slope has an inverse relation with the *SC*. In the first 55 km, the highest *SC* was 3.18 (1985), 1.38 (2000), and 1.28 (2015), while throughout the reach (within 150–160 km from the beginning), it was 4.67 with an altitude of about 20 m in 2015. As seen in Table 6, the highest *SC*s in 1985 and 2000 were 3.44 and 3.99, respectively, which were identified within the range of 205 to 212 km from the beginning at 11 m.

Table 6. Minimum, mean, and maximum amounts of SC in 1985, 2000, and 2015.

Sinuosity Coefficient	1985	2000	2015
Mean	1.7	1.72	1.77
Max	3.44	3.99	4.67
Min	1.02	1.04	1.06

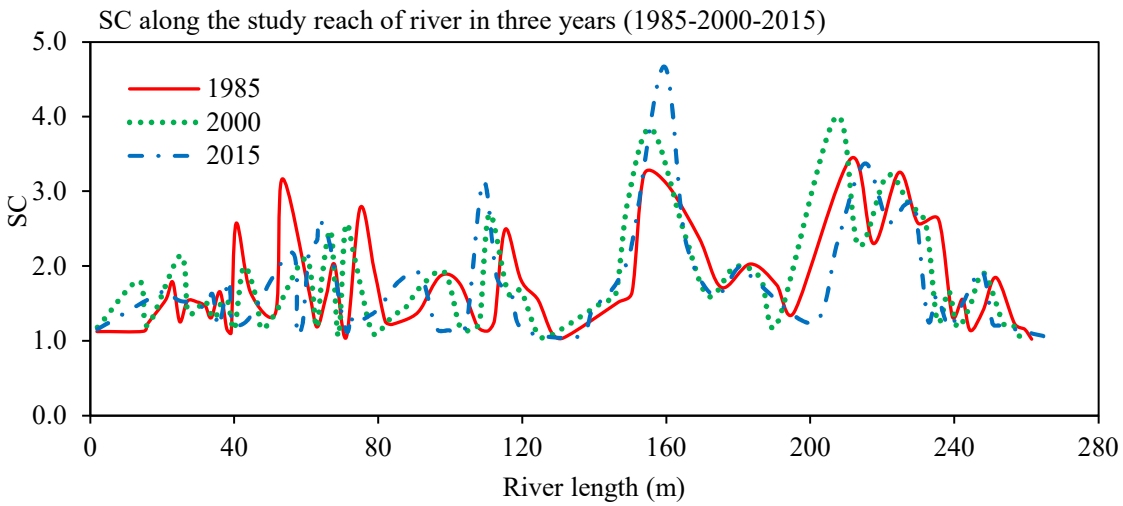

Figure 6. Local *SC* changes in the Karun River from Gotvand to Shirinshahr in 1985, 2000, and 2015.

As shown in Table 7, the meandering pattern appeared as the dominant morphological pattern at each time interval, whereas the arcs with the straight *SC* disappeared gradually. Additionally, the sinusoidal pattern was increased, and the meandering pattern was reduced to less than 2%. Although the upper limit of *SC* equals approximately three, the maximum *SC* of Karun (Table 6) in 1985, 2000, and 2015 was 3.44, 3.99, and 4.67, respectively. Our results are consistent with other studies such as Hoseynzade and Ismaili (2016) on Babol (3.62) and Talar River (3.04) in Iran and Kiss (2008) on Tisza River (more than 4) in Hungary. According to Figure A1, the *SC* increases as the altitude decreases. In addition, the river's migration capacity was minimized at high altitudes due to the mountainous texture and steep slopes; furthermore, as the river moves toward lower altitudes, the land's texture changes from the mountainous to the plain form and river migration increases.

Table 7. SC according to Leopold (1957) for the Karun River in 1985, 2000, and 2015.

Arc SC Index		1985			2000			2015		
		Number of Arcs	Arc Length (m)	Arc Length (%)	Number of Arcs	Arc Length (m)	Arc Length (%)	Number of Arcs	Arc Length (m)	Arc Length (%)
Straight	<1.05	3	6543	3.14	2	5095	2.5	-	-	-
Sinuous	1.06–1.3	17	35,024	16.79	19	42,848	21.01	19	42,171	21.56
Meander	>1.3	41	167,075	80.08	39	155,982	76.94	38	153,444	78.44
Total		61	208,642	100	60	203,925	100	57	195,615	100

3.3. Cornice Central Angle

Cornice's central angle was calculated for all arcs (Figure A2 (right panel) in Appendix A), and the percentage of meandering arcs of the Karun River was calculated for the studied time points (Table 8). As shown in Table 8, the central angles in the study area most frequently occurred within 85–158 degrees, related to the developed meandering category (70%, 73.5%, and 75% of arcs for 1985, 2000, and 2015, respectively). The second frequency was related to the non-developed meandering in all time intervals. Additionally, the lowest frequency in 1985 was related to 0–41 degrees (similar to meandering), which falls in the more developed meandering category (158–296) for 2000 and 2015. Additionally, according to Table 8, there is no case (central angle of arc) with more than 296 degrees and no more arcs from 2000 to 2015 in 0–41 degrees.

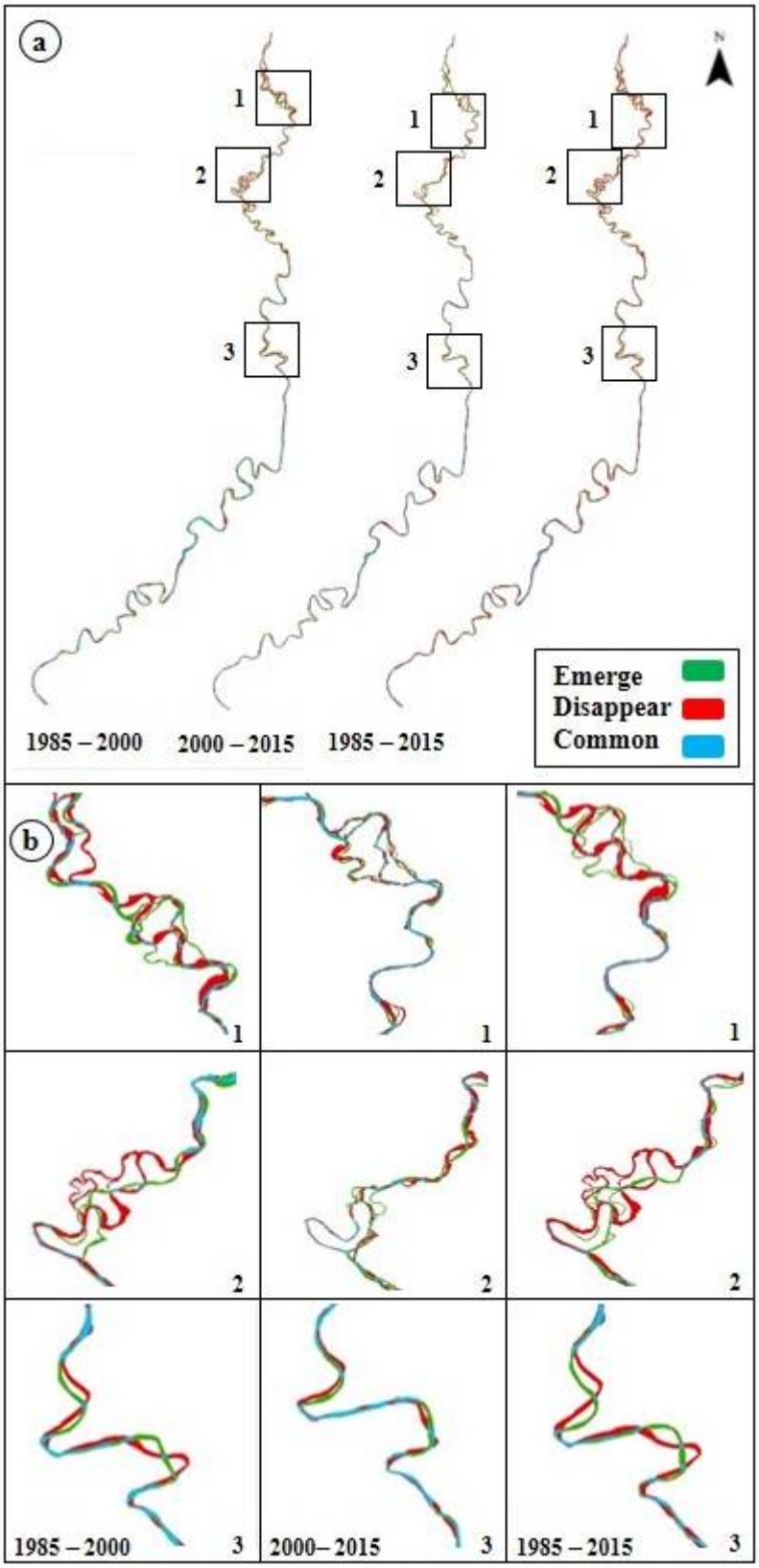

Figure 7. Plan morphological changes in Karun over 30 years: (**a**) Changes in the study area during three intervals shown at the bottom. (**b**) Zoomed-in view of 9 parts that are marked in (**a**).

Table 8. Rate of the meandering pattern in the Karun River based on the Cornice index in 1985, 2000, and 2015.

River Shape	Arc Central Angle (Degree)	Percentage		
		1985	2000	2015
Straight river	-	-	-	-
Semi-meandering river	0–41	1.4	0	0
Undeveloped meandering river	41–85	20	17.6	15.6
Developed meandering river	85–158	70	73.5	75
More developed meander-like river	158–296	8.6	8.8	9.4
River oxbow	>296	0	0	0

3.4. River Width

The results show that the river width reduced by 32% during the studied periods (Figure A2 (left panel) in Appendix A). The overall trend of the river's width showed widening towards the lower altitudes at the river's downstream, where the landscape changes from high altitudes to plain.

3.5. Stream Power

USP (Ω) was calculated for each arc along the river (Equation (7)), and its relation with the morphological factors (η_i) was explored. K_i and R^2 are coefficients of USP and determination (Equation (13)), respectively, presented in Table 9 and the last column is the general coefficient for each morphological parameter. The stream power per unit length has the most prediction ability for the morphological parameters. Since all the linear equations show a more than 88 percent correlation, it could be concluded that these equations are suitable for understanding the dynamic of morphological parameters using the power stream.

$$\eta_i = K_i \Omega \tag{13}$$

Table 9. Relationship between morphological parameters and unit stream power (k_i) and coefficient determination (r^2) in 1985, 2000, and 2015.

i	Years	1985		2000		2015		1985–2015
	η_i	k_i	R^2	k_i	R^2	k_i	R^2	k_i
1	Width, B	1.04	0.9792	0.9963	0.9915	1.0314	0.9535	0.9965
2	Wave Length, WL	0.9713	0.9962	0.9387	0.9915	0.9752	0.9945	0.9561
3	Cornice Central Angle, CA	1.0815	0.9477	1.048	0.9591	1.0628	0.889	0.9717
4	Sinuosity, Sin	1.0045	0.9884	0.9762	0.9962	0.9898	0.9851	0.9801

3.6. River Migration

The following results were obtained by comparing the river pattern in the study years. Figure 7 illustrates the trend of the river's dynamic. Part (a) shows the river changes from 1985–2000 and 2000–2015 and the changes that occurred from 1985–2015. Part (b) represents the trend of changes from 1985–2015. Figure 8 shows the spatiotemporal morphological evolution of the Karun River over space and time. The red parts are the dried and disappeared sections; the green color shows the emerging sections, and the blue part depicts the unaltered locations. Our results show that the river migrates gradually toward the east and southeast (Figure A3 in Appendix A), indicating that the river's east bank is unstable. Figure 8 shows the arcs with the most displacement along the Karun River reach (Gotvand to Shirinshahr). These changes indicate that the riverbanks in these arcs are unstable, so they need to be considered more than other parts. According to Figure 2 (right panel), agriculture and the built-up areas are the dominant land use. Therefore,

a sudden event such as heavy rain or flood could have many socio-economic consequences in the floodplain.

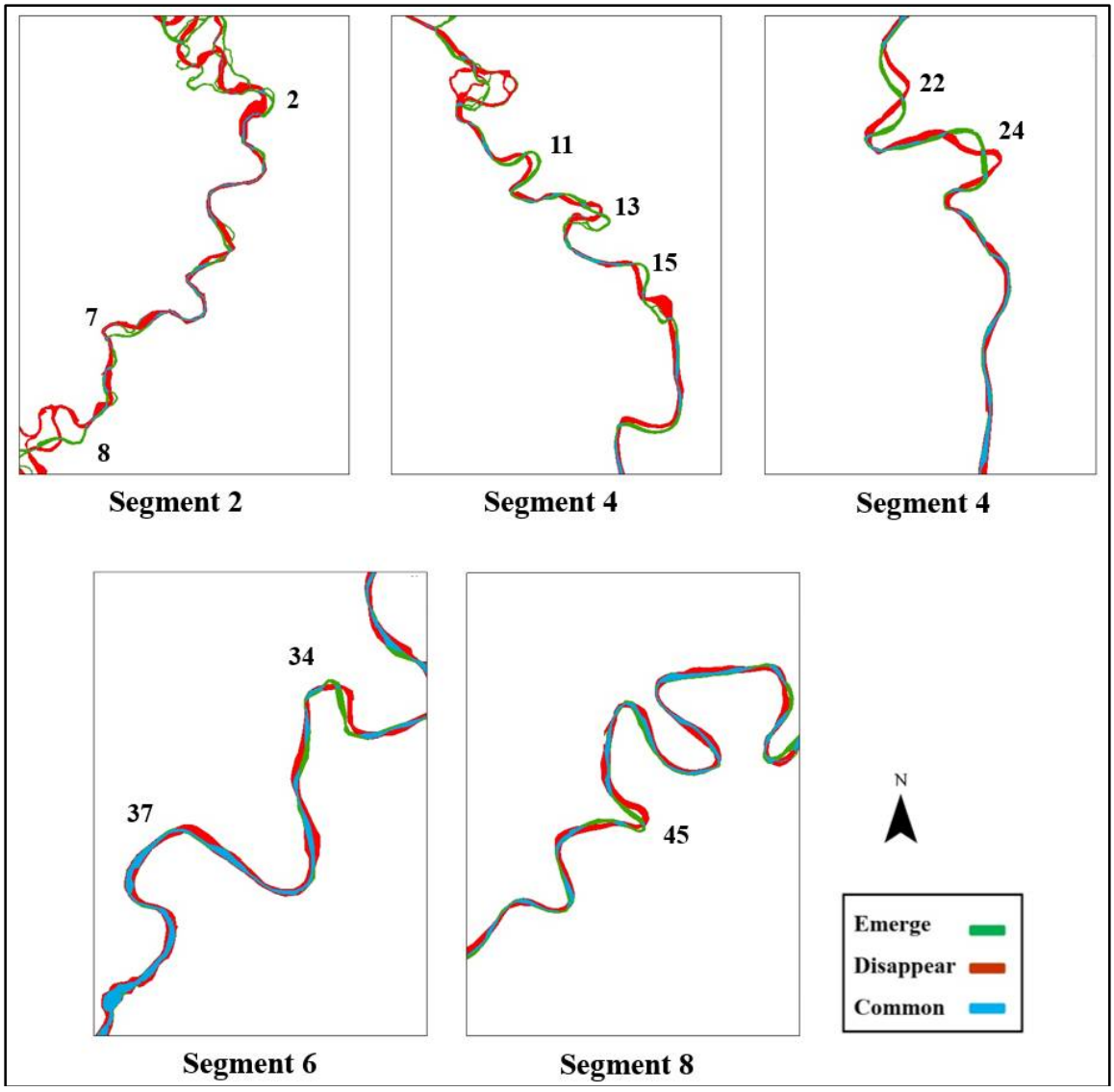

Figure 8. Arcs with most displacement along the Karun River (1985–2015).

3.7. Influence of Gotvand Dam on the Karun River Morphological Pattern

To investigate the influence of Gotvand Dam on the morphological changes in Karun River, the river path was examined in 1985, 2000, and 2015 and the common arcs (including 57 arcs for each year) were extracted (Table 10). Our exploration shows that the width of Karun River has decreased after the dam construction, which was expected due to the reduction and changes in the water and sediment discharge. However, sinuosity and Cornice central angle of more than half of the arcs in both periods have shown a positive change. For this specific case study, the percentage and type of changes for the curvature coefficient were almost the same both pre- and post-dam construction, whereas an increasing trend was observed for the changes in central angle of a positive type. As a result, the decrease in the river sediment and the increase in the river's channel erosion are consistent with the changes in sinuosity and Cornice central angle.

Table 10. The percentage (frequency) and type of morphological changes pre- and post-Gotvand Dam construction.

Time Interval	Relation Type	Width Changes (%)	Sinuosity Changes (%)	Cornice Changes (%)
1985–2000	Positive	26.42	56.6	52.83
	Negative	73.58	35.85	41.51
	Zero	0	7.55	5.66
2000–2015	Positive	22.64	56.6	62.26
	Negative	77.36	35.85	37.74
	Zero	0	7.55	0

4. Discussion

4.1. Influence of Human Activities on the River Morphology

This study investigated long-term morphological changes of the Karun River from downstream of Gotvand Dam to Shirinshahr (~300 Km). Gotvand Dam is one of the largest dams in Iran and the last downstream dam on the Karun River, which has led to changes in water and sediment volumes [44]. The average daily discharge of the river was 534 $m^3\ s^{-1}$ whereas, after the dam construction, it decreased to 490 $m^3\ s^{-1}$. The average daily suspended sediment loads before and after the dam construction were 16.36 and 9.12 gL^{-1}, respectively. Based on Equation (14), the river width directly relates to flow discharge and is inversely related to the sediment discharge. Therefore, decreasing the flow discharge of the Karun River can be a reason for the shrinkage in the river width, which is similar to the findings of Mengen et al. (2020) [54] on the Mekong River and Byishimo et al. (2014) [55].

$$W \cong 1.3Q^{0.62} d_{50}^{-0.15} Q_s^{-0.15} \quad (14)$$

Morphological changes happen gradually in uncontrolled rivers, but in rivers under human control, these changes occur in a shorter time. Dam construction, land use change, water transmission networks, urban development, sand mining, and bank protection are influential factors that accelerate river changes [56]. Therefore, humans play a crucial role in the river system, hence considering that they are an effective measure for a better realization of human–river interaction.

4.2. Morphological Pattern

According to Schumm's approach, the Karun River's reaches were divided into eight intervals; four sections have shown the meandering form, two of them belonged to the braided category, and the other two had straight form. The majority of the morphological changes happened in the first (braided pattern), third (braided pattern), and fourth intervals (meandering pattern), where cropland and residential area are the dominant land use in the floodplain (Figure 2—right panel) and river reach. Therefore, the sudden morphological changes in the river caused by extreme floods will affect human lives and property. On the other hand, the pattern of morphological changes indicated that the slope was inversely related to the river sinuosity, which conforms to the Timár flume experiments [57] and Petrovzszki and Frasson's research along natural rivers at any discharge value [48,58].

The number of river arteries decreased over time, where the flow and sediment discharge reduced after the construction of Gotvand Dam. Furthermore, adjacent arcs were interconnected over time and evolved into a single arc. Shrinkage of the river width is another observation within the 30 years from 1985 to 2015. The studies of Nelson et al. (2013) [59] on the Jackson Dam and its morphological effects on the Snake River have shown that some of the river's arteries were dried up by decreasing flow and sediment discharge. Most of the arc's movements occurred in Gotvand and Mollasani, indicating the greater slope and remarkable migration in the reach. It shows that the river tends to deplete its high energy through transverse displacement floodplain. Three ranges are highlighted in Figure 8, which had the most changes in the river reach during the study

period (1985–2015). They are also disposed to change in the future, which can be hazardous to cropland and residential areas.

The river's arrival into the plain provides a condition for morphological changes. Reduction in the slope and river velocity and changes in the texture of river reach are some potential reasons for the creation of the meandering form in the floodplain. Sinuosity coefficient, the river width, and central angle had an inverse relation with the slope, and by gentling the slope, their value increases, which is approved by Frasson et al [48].

Morphological parameters were calculated based on USP, making it possible to predict changes' feasibility before natural events such as floods. In this research, the prediction of morphological parameter changes based on USP has been studied and evaluated for the first time, which had an acceptable result. Human activities in the river reach and floodplains lead to changes in river morphology. When there is a good correlation between USP and morphological parameters, it indicates that the river eventually becomes a USP function.

5. Conclusions

This paper explored the long-term trend of the Karun River as the most important river of Iran and revealed that it evolved into a developed meandering system. Due to the decreasing amount of water discharge, some arteries were lost, the width of the river has decreased, and it turned into a single stream in line with the majority of previous studies. If the current trend continues, cropland and urban areas on the fragile parts of the river will be at high risk. In addition, since the river migrates toward the east and southeast, the east coastal lands of the river will be more susceptible to change. Additionally, the relevance of morphology parameters and stream power has been surveyed in this study, which helps to anticipate the possible alteration of morphological characteristics.

We suggest considering the influence of hydrological events such as extreme floods in recent years and other relevant variables such as soil texture and the riparian zone on the Karun River in future studies. Moreover, in the coming years, Sentinel-2 images can be considered as an alternative source due to their higher spatial resolution, which shows more details of spatial variations in river dynamics.

Author Contributions: All authors were involved in the production and writing of the manuscript. Conceptualization, S.A.A.; methodology, A.A.-F. and H.S.-M.; software, A.A.-F.; validation, S.A.A., A.A.-F. and H.S.-M.; formal analysis, A.A.-F. and H.S.-M.; investigation, A.A.-F. and S.A.A.; resources, H.M.; data curation, A.A.-F. and H.S.-M.; writing—original draft preparation, A.A.-F. and H.S.-M.; writing—review and editing, All authors; visualization, A.A.-F.; supervision, S.A.A., H.S.-M. and H.M.; project administration, S.A.A.; All authors have read and agreed to the published version of the manuscript.

Funding: This research received no external funding.

Institutional Review Board Statement: Not applicable.

Informed Consent Statement: Not applicable.

Data Availability Statement: Derived data supporting the findings of this study are available from the corresponding author on request.

Conflicts of Interest: The authors declare no conflict of interest.

Appendix A

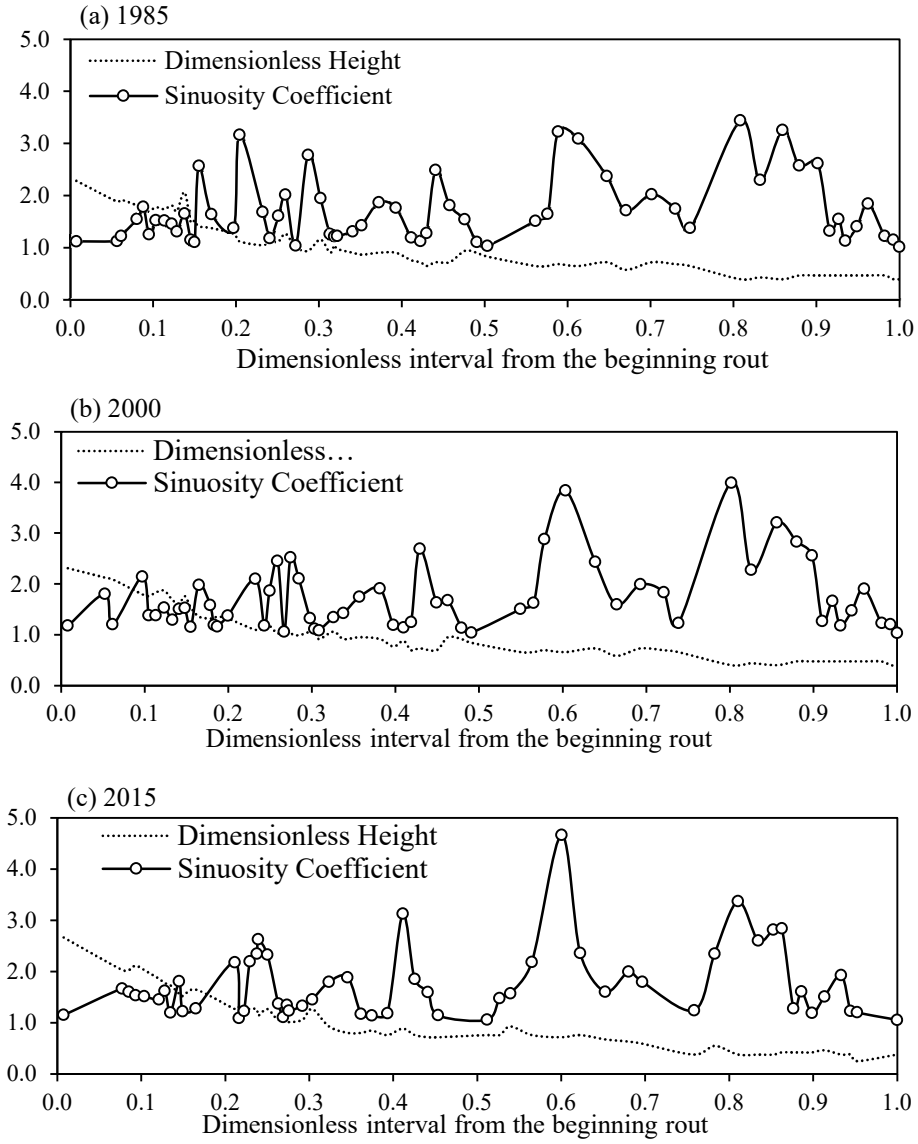

Figure A1. Simultaneous height and SC changes across the study region (1985, 2000, and 2015).

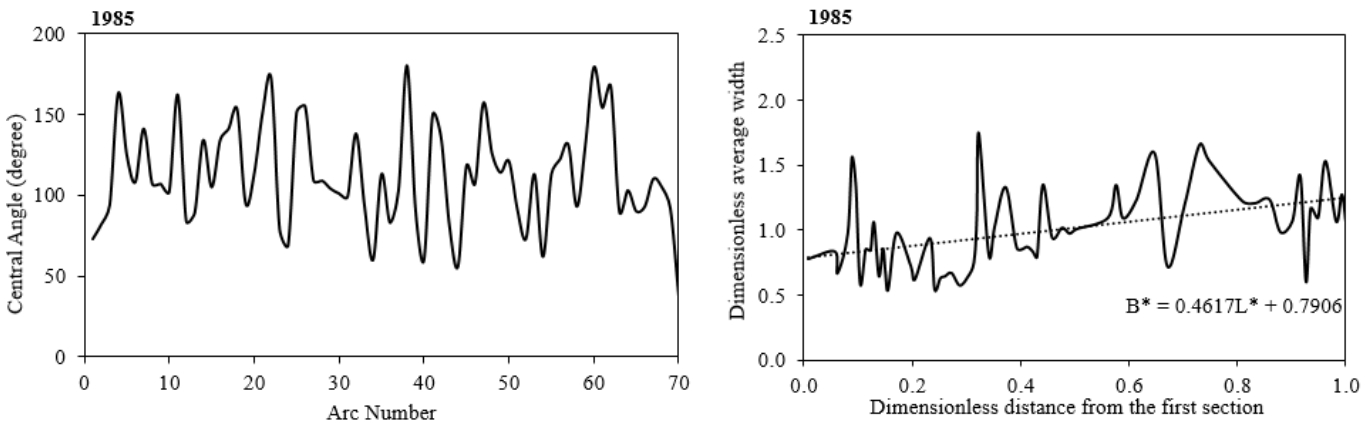

Figure A2. *Cont.*

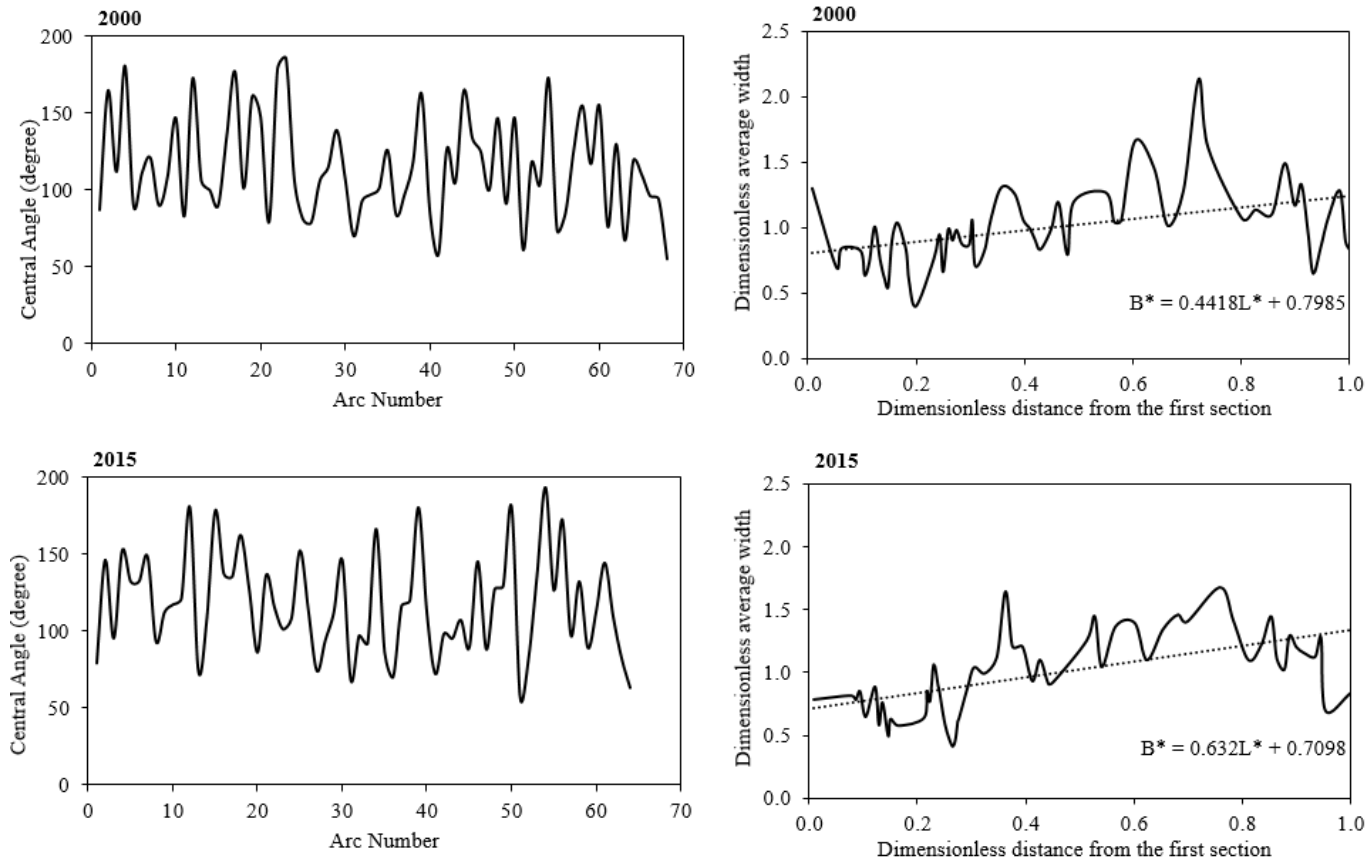

Figure A2. (**Right**) Cornice central angle graph of the study region in 1985, 2000, and 2015, and (**Left**) the process of changing the river width in the study region (1985, 2000, and 2015).

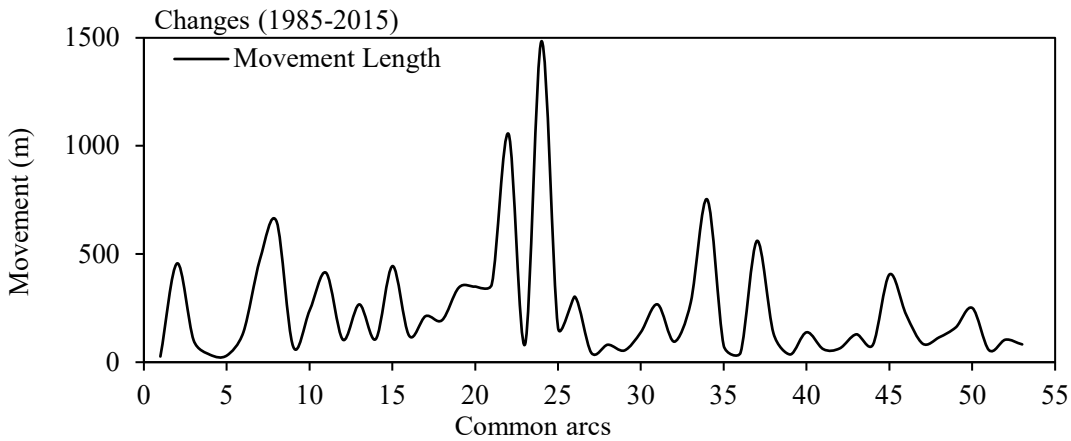

Figure A3. River displacement in common arcs.

References

1. Crosato, A. *Analysis and Modelling of River Meandering—Analyse En Modellering van Meanderende Rivieren*; IOS Press: Amsterdam, The Netherlands, 2008.
2. Muhar, S.; Jungwirth, M.; Unfer, G.; Wiesner, C.; Poppe, M.; Schmutz, S.; Hohensinner, S.; Habersack, H. 30 Restoring Riverine Landscapes at the Drau River: Successes and Deficits in the Context of Ecological Integrity. *Dev. Earth Surf. Process.* **2007**, *11*, 779–803. [CrossRef]
3. Rapp, C.F.; Abbe, T.B. *A Framework for Delineating Channel Migration Zones*; 03-06-027, Washington State Departments of Ecology and Transportation: Lacey, WA, USA, 2003.
4. Sarker, S.; Veremyev, A.; Boginski, V.; Singh, A. Critical Nodes in River Networks. *Sci. Rep.* **2019**, *9*, 11178. [CrossRef]

5. Lagasse, P.; Zevenbergen, L.; Spitz, W.; Thorne, C. Methodology for Predicting Channel Migration. Available online: https://nap.nationalacademies.org/read/23352/chapter/1 (accessed on 5 December 2021).
6. Perucca, E.; Camporeale, C.; Ridolfi, L. Influence of River Meandering Dynamics on Riparian Vegetation Pattern Formation. *J. Geophys. Res. Biogeosci.* **2006**, 111. [CrossRef]
7. Kong, D.; Latrubesse, E.M.; Miao, C.; Zhou, R. Morphological Response of the Lower Yellow River to the Operation of Xiaolangdi Dam, China. *Geomorphology* **2020**, *350*, 106931. [CrossRef]
8. Lofthouse, C.; Robert, A. Riffle-Pool Sequences and Meander Morphology. *Geomorphology* **2008**, *99*, 214–223. [CrossRef]
9. Camporeale, C.; Hydrology, L.R. Interplay among River Meandering, Discharge Stochasticity and Riparian Vegetation. *J. Hydrol.* **2010**, *382*, 138–144. [CrossRef]
10. Ghimire, S.; Higaki, D. Dynamic River Morphology Due to Land Use Change and Erosion Mitigation Measures in a Degrading Catchment in the Siwalik Hills, Nepal. *Int. J. River Basin Manag.* **2015**, *13*, 27–39. [CrossRef]
11. Morianou, G.G.; Kourgialas, N.N.; Karatzas, G.P.; Nikolaidis, N.P. Assessing Hydro-Morphological Changes in Mediterranean Stream Using Curvilinear Grid Modeling Approach—Climate Change Impacts. *Earth Sci. Inform.* **2017**, *11*, 205–216. [CrossRef]
12. Arróspide, F.; Mao, L.; Escauriaza, C. Morphological Evolution of the Maipo River in Central Chile: Influence of Instream Gravel Mining. *Geomorphology* **2018**, *306*, 182–197. [CrossRef]
13. Bregoli, F.; Crosato, A.; Paron, P.; McClain, M.E. Humans Reshape Wetlands: Unveiling the Last 100 years of Morphological Changes of the Mara Wetland, Tanzania. *Sci. Total Environ.* **2019**, *691*, 896–907. [CrossRef]
14. Yousefi, S.; Moradi, H.R.; Keesstra, S.; Pourghasemi, H.R.; Navratil, O.; Hooke, J. Effects of Urbanization on River Morphology of the Talar River, Mazandarn Province, Iran. *Geocarto Int.* **2019**, *34*, 276–292. [CrossRef]
15. Fernandes, M.R.; Aguiar, F.C.; Martins, M.J.; Rivaes, R.; Ferreira, M.T. Long-Term Human-Generated Alterations of Tagus River: Effects of Hydrological Regulation and Land-Use Changes in Distinct River Zones. *Catena* **2020**, *188*, 104466. [CrossRef]
16. Das, T.K.; Haldar, S.K.; Das Gupta, I.; Sen, S. River Bank Erosion Induced Human Displacement and Its Consequences. *Living Rev. Landsc. Res.* **2014**, *8*, 3. [CrossRef]
17. Gordon, E.; Meentemeyer, R.K. Effects of Dam Operation and Land Use on Stream Channel Morphology and Riparian Vegetation. *Geomorphology* **2006**, *82*, 412–429. [CrossRef]
18. Rutherfurd, I.; Price, P. Management on Stream Erosion. *Influ. Riparian Manag. Stream Eros.* **2007**, 86–116.
19. Liu, Y.; Qiao, Y.; Zhong, Y. Dynamic Monitoring and Driving Force Analysis on Rivers and Lakes in Zhuhai City Using Remote Sensing Technologies. *Procedia Environ. Sci.* **2011**, *10*, 2677–2683. [CrossRef]
20. Yousefi, S.; Khatami, R.; Mountrakis, G.; Mirzaee, S.; Pourghasemi, H.R.; Tazeh, M. Accuracy Assessment of Land Cover/Land Use Classifiers in Dry and Humid Areas of Iran. *Environ. Monit. Assess.* **2015**, *187*, 641. [CrossRef]
21. Sarker, S.; Sarker, T.; Raihan, S.U. Comprehensive Understanding of the Planform Complexity of the Anastomosing River and the Dynamic Imprint of the River's Flow: Brahmaputra River in Bangladesh. *Earth Sci. India* **2022**, *preprint*. [CrossRef]
22. Pal, S. Impact of Massanjore Dam on Hydro-Geomorphological Modification of Mayurakshi River, Eastern India. *Environ. Dev. Sustain.* **2016**, *18*, 921–944. [CrossRef]
23. Han, J.; Zhang, W.; Fan, Y.; Yu, M. Interacting Effects of Multiple Factors on the Morphological Evolution of the Meandering Reaches Downstream the Three Gorges Dam. *J. Geogr. Sci.* **2017**, *27*, 1268–1278. [CrossRef]
24. Reisenbüchler, M.; Bui, M.D.; Skublics, D.; Rutschmann, P. An Integrated Approach for Investigating the Correlation between Floods and River Morphology: A Case Study of the Saalach River, Germany. *Sci. Total Environ.* **2019**, *647*, 814–826. [CrossRef] [PubMed]
25. Can, M.; Çalışır, E.; Akpınar, A.; Doğan, E. The Effects of the Dam Construction Process on Downstream River Geomorphology. *Arab. J. Geosci.* **2021**, *14*, 2122. [CrossRef]
26. Sarasekanrood, S.A.; Madadi, A.; Bashokouh, Z.; Ghaleh, E.; Sciences, H.; Sciences, H. Investigating the Pattern and Dynamics of Gharasu River in Ardabil (From Samian Bridge to Sabalan Dam). *Hydrogeomorphology* **2021**, *8*, 2019–2022.
27. Khaleghi, S.; Sadough, S.H.; Khodayari, M. Assessment of Morphological Changes of Taleghan River in Upstream of Taleghan Dam. *Sustain. Earth Rev.* **2020**, *1*, 38–45. [CrossRef]
28. Sarker, S.; Sarker, S. Essence of MIKE 21C (FDM Numerical Scheme): Application on the River Morphology of Bangladesh. *Open J. Model. Simul.* **2022**, *10*, 88–117. [CrossRef]
29. Lecce, S.A. Stream Power, Channel Change, and Channel Geometry in the Blue River, Wisconsin. *Phys. Geogr.* **2013**, *34*, 293–314. [CrossRef]
30. Ramani, R.S.; Patel, P.L.; Timbadiya, P.V. Key Morphological Changes and Their Linkages with Stream Power and Land-Use Changes in the Upper Tapi River Basin, India. *Int. J. Sediment. Res.* **2021**, *36*, 602–615. [CrossRef]
31. Kleinhans, M.G.; Van Den Berg, J.H. River Channel and Bar Patterns Explained and Predicted by an Empirical and a Physics-Based Method. *Earth Surf. Process. Landf.* **2010**, *36*, 721–738. [CrossRef]
32. Candel, J.; Kleinhans, M.; Makaske, B.; Wallinga, J. Predicting River Channel Pattern Based on Stream Power, Bed Material and Bank Strength. *Prog. Phys. Geogr. Earth Environ.* **2020**, *45*, 253–278. [CrossRef]
33. Woolderink, H.A.G.; Cohen, K.M.; Kasse, C.; Kleinhans, M.G.; Van Balen, R.T. Patterns in River Channel Sinuosity of the Meuse, Roer and Rhine Rivers in the Lower Rhine Embayment Rift-System, Are They Tectonically Forced? *Geomorphology* **2021**, *375*, 107550. [CrossRef]

34. Ollero, A. Channel Changes and Floodplain Management in the Meandering Middle Ebro River, Spain. *Geomorphology* **2010**, *117*, 247–260. [CrossRef]
35. Yousefi, S.; Vfakhah, M.; Mirzaee, S.; Tavangar, S. Changes of Some Morphological Parameters of Karoon River Using Remote Sensing. *Iran. Remot Sens. GIS* **2013**, *5*, 85–96.
36. Khoi, D.N.; Suetsugi, T. Impact Des Changements Climatiques et de l'utilisation Des Terres Sur Les Processus Hydrologiques et La Production de Sédiments-Étude de Cas Du Bassin Versant de La Rivière Be, Vietnam. *Hydrol. Sci. J.* **2014**, *59*, 1095–1108. [CrossRef]
37. Bhuiyan, M.A.H.; Kumamoto, T.; Suzuki, S. Application of Remote Sensing and GIS for Evaluation of the Recent Morphological Characteristics of the Lower Brahmaputra-Jamuna River, Bangladesh. *Earth Sci. Informatics* **2014**, *8*, 551–568. [CrossRef]
38. Aiello, A.; Adamo, M.; Canora, F. Remote Sensing and GIS to Assess Soil Erosion with RUSLE3D and USPED at River Basin Scale in Southern Italy. *Catena* **2015**, *131*, 174–185. [CrossRef]
39. Clerici, A.; Perego, S.; Chelli, A.; Tellini, C. Morphological Changes of the Floodplain Reach of the Taro River (Northern Italy) in the Last Two Centuries. *J. Hydrol.* **2015**, *527*, 1106–1122. [CrossRef]
40. Mitidieri, F.; Papa, M.N.; Amitrano, D.; Ruello, G. European Journal of Remote Sensing River Morphology Monitoring Using Multitemporal SAR Data: Preliminary Results. *Eur. J. Remote Sens.* **2017**, *49*, 889–898. [CrossRef]
41. Hemmelder, S.; Marra, W.; Markies, H.; De Jong, S.M. Monitoring River Morphology & Bank Erosion Using UAV Imagery—A Case Study of the River Buëch, Hautes-Alpes, France. *Int. J. Appl. Earth Obs. Geoinf.* **2018**, *73*, 428–437. [CrossRef]
42. Zheng, S.; Han, S.; Tan, G.; Xia, J.; Wu, B.; Wang, K.; Edmonds, D.A. Morphological Adjustment of the Qingshuigou Channel on the Yellow River Delta and Factors Controlling Its Avulsion. *Catena* **2018**, *166*, 44–55. [CrossRef]
43. Nones, M. Remote Sensing and GIS Techniques to Monitor Morphological Changes along the Middle-Lower Vistula River, Poland. *Int. J. River Basin Manag.* **2021**, *19*, 345–357. [CrossRef]
44. Rashidi, M.; Hoseinzade, S.R.; Sepehr, A.; Zarei, H.; Khanebad, M. The Study of Geomorphological Changes in Karun River and Its Reasons in the Period of 1954–2011(1334–1391). *Quant. Geomorphol. Res.* **2016**, *5*, 43–59.
45. Arshad, S.; Morid, S.; Hadi, M. Assessing the Trend of Morphologic Changes of Rivers Using Remote Sensing (Case Study: Karun river between Gotvand and Farsiat). *J. Agric. Sci. Nat. Resour.* **2007**, *14*, 180–194.
46. Xu, H. Modification of Normalised Difference Water Index (NDWI) to Enhance Open Water Features in Remotely Sensed Imagery. *Int. J. Remote Sens.* **2007**, *27*, 3025–3033. [CrossRef]
47. Maghsoudi, M.; Zamanzadeh, S.M.; Yamani, M.; Hajizadeh, A.; Maghsoudi, M.; Zamanzadeh, S.M.; Yamani, M.; Hajizadeh, A. Morphometric Assessment of Meandering River in Arid Region Using Improvement Model (Case Study: Maroon River). *J. Water Resour. Prot.* **2017**, *9*, 358–377. [CrossRef]
48. Frasson, R.P.d.M.; Pavelsky, T.M.; Fonstad, M.A.; Durand, M.T.; Allen, G.H.; Schumann, G.; Lion, C.; Beighley, R.E.; Yang, X. Global Relationships Between River Width, Slope, Catchment Area, Meander Wavelength, Sinuosity, and Discharge. *Geophys. Res. Lett.* **2019**, *46*, 3252–3262. [CrossRef]
49. Leopold, A. *Plant Growth and Development*; McGraw-Hill Book Co.: New York, NY, USA, 1964.
50. Morisawa, M. *Rivers: Form and Process*; Clayton, K., Ed.; Longman: London, UK; New York, NY, USA, 1985.
51. Selby, M.J. *Earth's Changing Surface: An Introduction to Geomorphology*; Oxford University Press: Oxford, UK, 1985.
52. Brierley, G.; Fryirs, K. *Geomorphology and River Management: Applications of the River Styles Framework*; Wiley-Blackwell: Hoboken, NJ, USA, 2005.
53. Schumm, S.A. Patterns of Alluvial Rivers. *Annu. Rev. Earth Planet. Sci.* **1985**, *13*, 5–27. [CrossRef]
54. Mengen, D.; Ottinger, M.; Leinenkugel, P.; Ribbe, L. Modeling River Discharge Using Automated River Width Measurements Derived from Sentinel-1 Time Series. *Remote Sens.* **2020**, *12*, 3236. [CrossRef]
55. Byishimo, P.; Vargas-Luna, A.; Crosato, A. Effects of Variable Discharge on the River Channel Width Variation. Available online: https://www.researchgate.net/publication/275339519_Effects_of_variable_discharge_on_the_river_channel_width_variation (accessed on 5 December 2021).
56. Wang, P.; Fu, K.; Huang, J.; Duan, X.; Yang, Z. Morphological Changes in the Lower Lancang River Due to Extensive Human Activities. *PeerJ* **2020**, *8*, e9471. [CrossRef]
57. Timár, G. Controls on Channel Sinuosity Changes: A Case Study of the Tisza River, the Great Hungarian Plain. *Quat. Sci. Rev.* **2003**, *22*, 2199–2207. [CrossRef]
58. Petrovszki, J. Is Sinuosity a Function of Slope and Bankfull Discharge? —A Case Study of the Meandering Rivers in the Pannonian Basin. *Hydrol. Earth Syst. Sci. Discuss.* **2014**, *11*, 12271–12290. [CrossRef]
59. Nelson, N.C.; Erwin, S.O.; Schmidt, J.C. Spatial and Temporal Patterns in Channel Change on the Snake River Downstream from Jackson Lake Dam, Wyoming. *Geomorphology* **2013**, *200*, 132–142. [CrossRef]